The International Society of Precision Agriculture presents the

15th International Conference on
Precision Agriculture
26–29 JUNE 2022
Minneapolis Marriott City Center | Minneapolis, Minnesota USA

Nitrogen status prediction in pasture fields using visible light UAV data combined with Sentinel-2 images

Francisco R. da S. Pereira [a,b,1*], Joaquim P. de Lima[c], Rodrigo G. Freitas[c], Aliny A. Dos Reis[b], Lucas R. do Amaral[c], Gleyce K. D. A. Figueiredo[c], Rubens A. C. Lamparelli[b], Juliana C. Pereira[a], Paulo S. G. Magalhães[b]

[a]Federal Institute of Education, Science and Technology of Alagoas, 57120-000, Satuba, Alagoas, Brazil

[b]Interdisciplinary Centre of Energy Planning, University of Campinas, 13083-896, Campinas, São Paulo, Brazil

[c]School of Agricultural Engineering, University of Campinas, 13083-875, Campinas, São Paulo, Brazil

[d]Embrapa Agricultural Informatics, Brazilian Agricultural Research Corporation, 13083-886, Campinas, São Paulo, Brazil

[e]University of West Paulista, 19050-920, Presidente Prudente, São Paulo, Brazil

[1]Permanent address: Federal Institute of Education, Science and Technology of Alagoas, 57120-000, Satuba, Alagoas, Brazil

*Corresponding author - rafael.pereira@ifal.edu.br

A paper from the Proceedings of the
15th International Conference on Precision Agriculture
June 26-29, 2022
Minneapolis, Minnesota, United States

Abstract.

Pasture fields under an integrated crop-livestock system (ICLS) usually receive low or no nitrogen (N) fertilization rates since the expectation is that nitrogen demand will be provided by the remaining soybean straw previously cropped. However, maintaining suitable field N levels is the key to achieving sustainability in agricultural production systems. In this sense, remote sensing technologies play an essential role in N pasture monitoring. With the launch of the Sentinel-2 missions (free imagery and high spectral resolution), new opportunities have arisen for nitrogen status monitoring. Additionally, low-cost UAV sensors that explore the RGB spectrum are employed for agricultural monitoring. However, few studies have investigated the combination of UAVs and satellite information to assess nitrogen status variability. Thus, to estimate the nitrogen variability in pasture fields under an ICLS, we tested the performance of exclusively visible light UAV data (i.e., RGB – red, green, and blue), named UAV_RGB and Sentinel-2 data (both individually and combined), to monitor plant N content (PNC), aboveground biomass (AGB), and

nutritional nitrogen index (NNI). The study area had 200 hectares in the western region of São Paulo State, Brazil. During the forage (*Urochloa ruziziensis*) growing season, we conducted three field campaigns to collect data, obtaining 116 samples. We used the original bands from UAV_RGB and Sentinel-2 and various vegetation indices (VIs) to capture the vegetation conditions during the study period. The assessment of PNC, AGB, and NNI employed the root mean square error (RMSE), mean absolute error (MAE) in absolute and percentage terms, the coefficient of determination (R2), and the RMSE-observations standard deviation ratio (RSR) to evaluate and compare the random forest model performance. The UAV visible data combined with the Sentinel-2 data were complementary and benefited each other in the N estimation (RSR < 0,7). The combination of data overcame the individual performance. Therefore, we concluded that using UAV_RGB data with multispectral Sentinel-2 data is more efficient for monitoring nitrogen variability in commercial pasture fields.

Proceedings of the 15th International Conference on Precision Agriculture
June 26-29, 2022, Minneapolis, Minnesota, United States

2

Introduction

Nitrogen (N) is one of the most demanded elements in agricultural production, whose deficiency reduces yield, and overapplication has undesirable environmental and financial impacts. Monitoring N status has been a challenge even in pastures cultivated under integrated crop-livestock systems (ICLSs), in which soybean-pasture succession allows nitrogen recovery to forage grass coverage. Commonly, chemical laboratory analysis is necessary to quantify plant nitrogen content (PNC), which, associated with aboveground biomass (AGB), provides the nutritional nitrogen index (NNI). Therefore, frequent field monitoring becomes impracticable due to appropriate time and costs (Vigneau et al. 2011).

Remote sensing by unmanned aerial vehicles (UAVs) or satellites is one of the most prominent strategies to monitor N status in plants. However, outstanding N predictions usually demand high sensor specifications, such as infrared bands and high spatial resolutions. Such specifications are commonly present on multispectral cameras boarded on UAVs or commercial satellites, which are expensive and impracticable to most farmers. On the other hand, low-cost cameras (red, green, and blue – RGB) and free satellite images, such as Sentinel 2, are exciting alternatives. The high spatial resolution and broad spectral resolution present on the sensors can be essential for N prediction. We hypothesized that the high spatial resolution provided by UAVs could overcome the absence of near-infrared region bands in RGB sensors, and the high spectral resolution from Sentinel 2 (red, green, blue, red-edge, near infrared, and shortwave infrared) could compensate for its broad spatial resolution. Furthermore, the association data of both platforms would benefit from the advantages of each platform individually.

Thus, in this study, we assessed the performance of visible bands camera boarded on unmanned aerial vehicle (UAV_RGB) and Sentinel2A platforms to monitor plant N content (PNC), aboveground biomass (AGB), and nutritional nitrogen index (NNI) in pasture fields under an Integrated Crop-Livestock System. We also evaluated whether combining the remote sensing platform data improves prediction accuracy.

Materials and methods

The study area has 200 ha on a commercial farm located in the western region of São Paulo State, Brazil (21°38'4.64" S, 51°54'15.65" W, 338 m above sea level) (Figure 1). The soil is predominantly sandy loam, Ultisol type (Soil Survey Staff, 2014). The climatic conditions correspond to Köppen's climatic type Aw, with a summer rainy season (i.e., December-March), where the mean annual rainfall ranges from 1,200 mm to 1,400 mm (Alvares et al. 2013). We used a local meteorological station to register the climatic information during field data collection (Figure 2). Between 2019 July and November, the average temperature was 23.8°C, and the accumulated rainfall was equal to 132.6 mm (Figure 2). The ICLS of soybean-pasture succession began in 2018. Soybean cultivation occurred during the summer season, and the pasture (*Pennisetum glaucum* and *Urochloa ruziziensis consortium*) was cultivated from April 2019 to November 2019. This study focused on assessing the nitrogen status in pasture fields with *Urochloa ruziziensis* grass, the most commonly used grass in ICLSs in Brazil, which entirely covered pasture fields after July.

We collected 116 field data samples on July 13th (35 samples), August 11th (38 samples), and November 4th (34 samples) during the forage growing season. A square frame of 1m$^{21\ m2}$ limited the area to collect biomass. We used white paper to limit the vertices before UAV flight, ensuring field measurements and images representing the same area. All the aboveground biomass (AGB) was collected and dried at $65\,°C$ to constant weight. The dry mass weight was registered to determine the dry mass (Mg ha^{-1}) and then ground to evaluate the plant nitrogen content (PNC) in the laboratory (Kjeldahl method). The nitrogen nutrition index (NNI) was calculated by the PNC and AGB ratio, according to equations (1) and (2) (Gastal et al. 2015).

$$NNI = \frac{Na}{Nc} \tag{1}$$

Proceedings of the 15th International Conference on Precision Agriculture
June 26-29, 2022, Minneapolis, Minnesota, United States

3

where Na = PNC in % (value in g kg^{-1} divided by 10) and

$$Nc = aW^b \qquad (2)$$

where a = 3.6 and b = 0.34 (as constants for tropical grasses) and W = AGB value (dry mass) in Mg ha^{-1}.
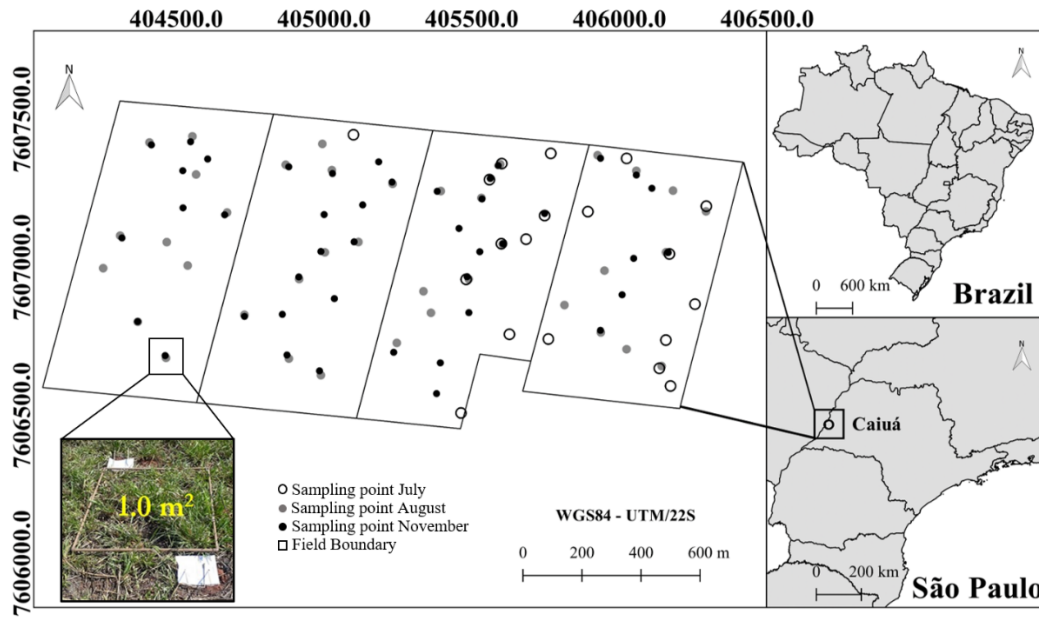

Figure 1. Experimental location and spatial distribution of the sampling points by field data collection.
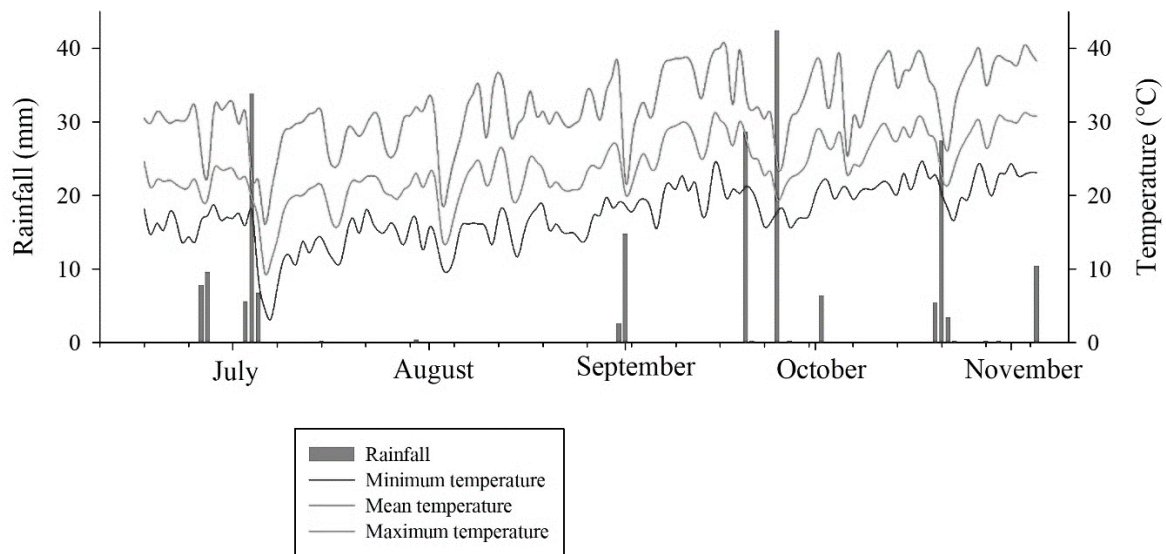

Figure 2 - Rainfall and temperatures during the period under study.

Sentinel 2A and UAV data collection

We used cloud-free surface images of the study area from Sentinel 2 level-2A (Sentinel2A) on July 10th, August 11th, and November 4th, 2019. The Sentinel2A bands used were blue (459.4–525.4 nm), green (541.8–577.8 nm), red (649.1–680.1 nm), and NIR (779.8–885.8 nm) bands with 10 m spatial resolution and red-edge1 (RE1) (696.6–711.6 nm), red-edge2 (RE2) (733–748 nm), red-edge3 (RE3) (772.8–792.8 nm), red-edge4 (RE4) (854.2–875.2 nm), shortwave infrared 1 (SWIR1)) (1568.2–1659.2 nm) and SWIR2 (2114.9–2289.9 nm) bands with 20 m resolution

Proceedings of the 15th International Conference on Precision Agriculture
June 26-29, 2022, Minneapolis, Minnesota, United States

4

(ESA, 2020).

UAV images were acquired at the same field data collection using a quadricopter (model G-Q45, G-drones) with a multispectral sensor (Rededge TM, Micasense, Seattle, Washington, USA), flying 115 m above ground from 13:00 to 17:00 GMT always under clear-sky conditions. We considered only the sensor visible bands (UAV_RGB): blue (465–485 nm), green (550–570 nm), and red (663–673 nm) for this study. The camera was set up to 75% overlap and sidelap, and the automatic flight control ensured parallel paths resulting in a ground sample distance (GSD) of 0.08 m. The UAV data spatial resolution was subsequently resampled to 1.0 m, calculating the mean of all pixels within the plot sample area. Pilots (researchers) and the UAV fulfilled the current local legislation. We used Agisoft Metashape® to process mosaics of every field campaign.

Statistical analysis and data mining

The complete dataset was composed of 116 samples of target variables (PNC, AGB, and NNI) and predictor variables (vegetation indices (VIs) (Appendix a) and original bands (OBs)). The predictor variable compositions were UAV_RGB: 5 VIs and 3 OBs, Sentinel2A: 51 VIs and 9 OBs, and the combined UAV_RGB + Sentinel2A (UAV_RGB+S2A): 56 Vis and 12 OBs. We randomly split the PNC, AGB, and NNI datasets between the training set (70%) and the test set (30%) per field data collection, ensuring data from the three periods for training and test datasets. Both sets were described and analyzed to determine the mean, median, minimum, maximum, and coefficient of variation (CV %). The Shapiro–Wilk test ($p<0.05$) showed no normality of the target variable distribution for the training and test sets. No significant difference was revealed (tNC = 0.110 and pNC=0912 ns; tBio = -0.536 and pBio = 0.593 ns; tNU = 0.211 and pNU=0.833 ns) by Student's t test (Viana et al. 2012), indicating suitable datasets. The attribute correlation was assessed by the Spearman method.

We used the nonparametric random forest (RF) technique to predict PNC, AGB, and NNI. Models based on regression trees (CART) generate sets of trees from a random independent raffle of the predictor subset of attributes (Breiman 2001). RF is a simple technique suitable for dealing with noise and outliers that informs measures of errors and importance (Breiman 2001). We used the Random Forest R package (Liaw et al., 2002), tuning the hyperparameter instance number per node and attribute number per tree. After cross-validation k-fold=10, we selected hyperparameters that resulted in lower errors.

Model performances were compared through mean absolute error (MAE) in absolute and percentage terms; root squares mean error (RSME) in absolute and percentage terms; coefficient of determination (R2); and RMSE-observation standard deviation ratio (RSR) in absolute terms. The RSR, proposed by Moriasi et al. (2007), rated RF models' performance using the following scale: very good ($0.00 \leq RSR \leq 0.50$), good ($0.50 < RSR \leq 0.60$), satisfactory ($0.60 < RSR \leq 0.70$) and unsatisfactory ($RSR > 0.70$). RSR is calculated through equation (3). We also generated prediction maps of PNC, AGB, and NNI for a subset area of 10 hectares within the study area to evaluate the effect on the spatial variability.

$$RSR = \frac{RMSE}{SD_{Obs}} \tag{3}$$

where RMSE = root squares mean error and SD_{Obs} = standard deviation observed.

Results and discussion

The UAV_RGB, Sentinel-2A, and combined UAV_RGB+S2A performances resulted in exciting differences in the PNC, AGB, and NNI estimates. The UAV_RGB data resulted in the lowest errors and the highest R² in PNC and AGB, while the UAV_RGB+S2A showed superiority in NNI (Table 1). It is worth mentioning that NNI quantifies the N status and indicates a deficiency or excessive consumption of N by the plants, helping farmers decide about N nutrition (Gastal et al.

**Proceedings of the 15th International Conference on Precision Agriculture
June 26-29, 2022, Minneapolis, Minnesota, United States**

5

2015). Therefore, we highlighted the results of UAV_RGB+S2A. On the other hand, Sentinel2A presented the lowest R², despite its excellent spectral resolution. This can be attributed to the worse spatial resolution.

Table 1- Mean absolute error (MAE), root-mean-square error (RMSE), and coefficient of determination (R²) of the random forest models using visible light unmanned aerial vehicle individual data (UAV_RGB), Sentinel2A individual data, and the data combination derived from two platforms (UAV_RGB + Sentinel2A) in the PNC (plant N content), AGB (aboveground biomass) and NNI (nitrogen nutrition index) predictions.

Platform	MAE		RMSE		R²
PNC					
	g kg⁻¹	%	g kg⁻¹	%	
UAV_RGB	2.05	20.15	3.00	29.54	0.65
Sentinel2A	2.19	21.59	3.24	31.96	0.53
UAV_RGB + Sentinel2A	2.11	20.77	3.09	30.43	0.60
AGB					
	Mg ha⁻¹	%	Mg ha⁻¹	%	
UAV_RGB	0.29	16.56	0.40	23.09	0.65
Sentinel2A	0.34	19.19	0.49	27.88	0.46
UAV_RGB + Sentinel2A	0.32	18.10	0.46	26.28	0.53
NNI					
		%		%	
UAV_RGB	0.07	20.73	0.09	28.14	0.46
Sentinel2A	0.07	21.69	0.10	30.34	0.32
UAV_RGB + Sentinel2A	0.06	17.87	0.08	23.43	0.69

We notice that UAV_RGB+S2A performed better than the individual UAV_RGB or Sentinel2A models by the RSR rating, reaching satisfactory classification (0.60 < RSR ≤ 0.70) for the three target variables (PNC, AGB, and NNI) (Figure 3). The UAV_RGB's very high spatial resolution and the bands relevant to N estimates from Sentinel 2A, especially NIR and RE, likely improved the model prediction accuracy from the two combined platforms' data.

In the prediction maps for the 10 ha in the study area, the PNC differences among the three models are notable (Figure 4). The significant details in the map generated from the spatial resolution of UAV_RGB represent difficulties in deploying nitrogen fertilization using the present machines. A feasible PNC map is reached by combining the Sentinel2A data (UAV_RGB+S2A). The spatial resolution range is also well represented by AGB and NNI from UAV_RGB+S2A. We noticed low NNI values representing N deficiency in the pasture. The N from the previous soybean straw did not provide pasture demand during the production season.
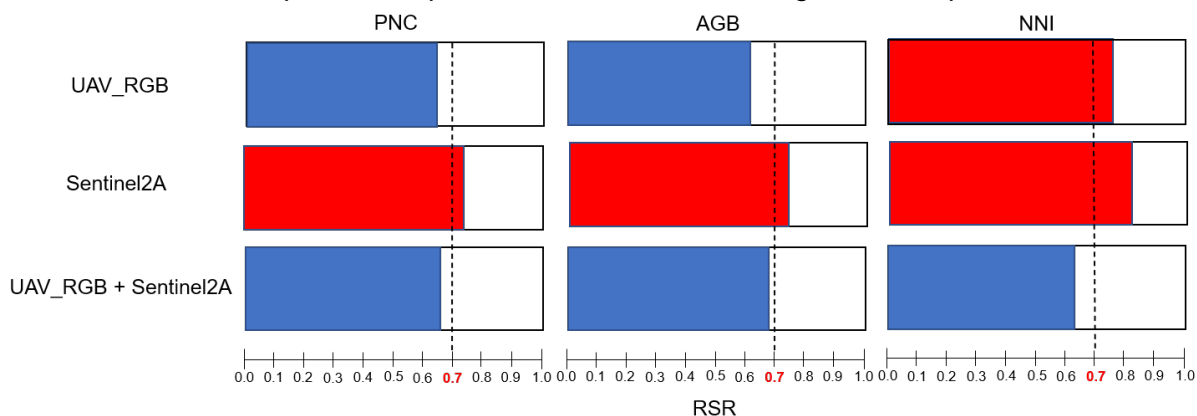

Figure 3. Visible light unmanned aerial vehicle data (UAV_RGB), Sentinel2A data, and the data combination derived from two platforms (UAV_RGB+S2A) in predicting PNC (plant N content), AGB (aboveground biomass), and NNI (nitrogen nutrition index) based on the RSR (RMSE-observation standard deviation ratio) classification. The blue color represents satisfactory RSR classification (0.60 < RSR ≤ 0.70), and the red color represents unsatisfactory RSR classification (RSR > 0.70).

Proceedings of the 15th International Conference on Precision Agriculture
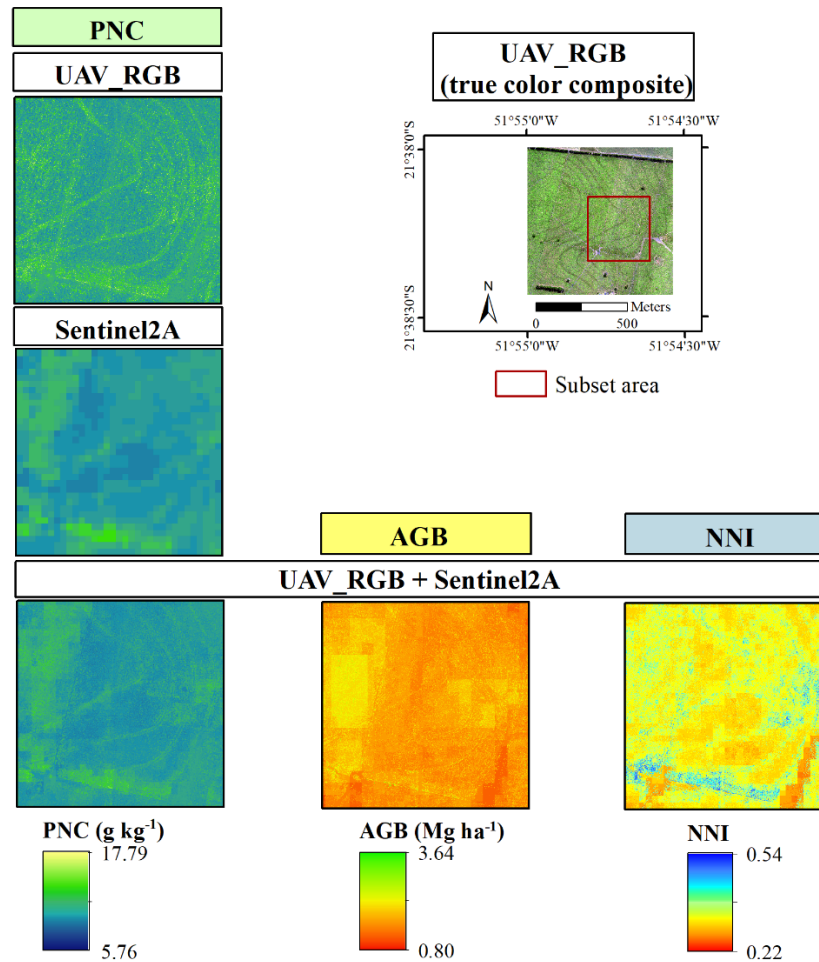**June 26-29, 2022, Minneapolis, Minnesota, United States**

6

Figure 4. Prediction maps obtained using the location of the selected subset (10 ha) in the study area for PNC (plant N content) obtained using visible light unmanned aerial vehicles data (UAV_RGB), Sentinel2A data, and the data combination derived from the two platforms (UAV_RGB+S2A); for AGB (aboveground biomass) and NNI (nitrogen nutrition index) obtained using the data combined (UAV_RGB+S2A).

Conclusion

Combining data from a visible light camera onboard an unmanned aerial vehicle and the Sentinel2A satellite (UAV_RGB+S2A) adds relevant information to improve the prediction of nitrogen parameters and guide appropriate fertilization in pasture fields under an integrated crop-livestock system. This approach is an attractive application due to the low financial cost of acquiring both images.

Further research is necessary to assess the combining UAV_RGB+S2A data to predict N status variability under different plant coverage, soil, and weather conditions.

Acknowledgments

References

Alvares, C. A., Stape, J. L., Sentelhas, P. C., De Moraes Gonçalves, J. L., & Sparovek, G. (2013).

Proceedings of the 15th International Conference on Precision Agriculture
June 26-29, 2022, Minneapolis, Minnesota, United States

7

Köppen's climate classification map for Brazil. *Meteorologische Zeitschrift*, *22*(6), 711–728. https://doi.org/10.1127/0941-2948/2013/0507

Breiman, L. (2001). (impo)Random forests(book). *Machine learning*, 5–32. https://doi.org/10.1023/A:1010933404324

Gastal, F., Lemaire, G., & Durand, J. (2015). *Improve Nitrogen-Use Efficiency*. *Crop Physiology* (Second Edi.). Elsevier Inc. https://doi.org/10.1016/B978-0-12-417104-6/00008-X

Lemaire, G., & Gastal, F. (1997). N Uptake and Distribution in Plant Canopies. *Diagnosis of the Nitrogen Status in Crops*, 3–43. https://doi.org/10.1007/978-3-642-60684-7_1

Moriasi, D. N., Arnold, J. G., Van Liew, M. W., Bingner, R. L., Harmel, R. D., & Veith, T. L. (2007). Model evaluation guidelines for systematic quantification of accuracy in watershed simulations. *American Society of Agricultural and Biological Engineers*, *50*(3), 885–900.

Vigneau, N., Ecarnot, M., Rabatel, G., & Roumet, P. (2011). Potential of field hyperspectral imaging as a non destructive method to assess leaf nitrogen content in Wheat. *Field Crops Research*, *122*(1), 25–31. https://doi.org/10.1016/j.fcr.2011.02.003

Nomenclature

AGB	aboveground biomass
ICLS	integrated crop-livestock system
N	nitrogen
NIR	near-infrared
NNI	nutritional nitrogen index
OBs	original spectral bands
RE	red-edge
RF	random forest
RGB	visible wavelengths – red, green, and blue
RMSE	root-mean-square error
SWIR	shortwave infrared
UAV	unmanned aerial vehicle
UAV_RGB	visible dataset (OBs+VIs) from UAV
UAV_RGB+S2A	Combined dataset from UAV_RGB and Sentinel2A
VIs	vegetation indices

Appendix

Appendix (a). Vegetation indices (VIs) derived from unmanned aerial vehicle visible lights (UAV_RGB) and Sentinel2A used in this study.

Quantity	Vegetation Index	*Equation	Platform	
1	GLI Green leaf index	(2Rgreen − Rred − Rblue)/(2Rgreen + Rred + Rblue)	UAV_RGB	Sentinel2A
2	NGRDI Normalized green red difference index	(Rgreen – Rred)/(Rgreen + Rred)	UAV_RGB	Sentinel2A
3	NPCI	(Rred − Rblue)/(Rred + Rblue)	UAV_RGB	Sentinel2A

Proceedings of the 15th International Conference on Precision Agriculture
June 26-29, 2022, Minneapolis, Minnesota, United States

8

	Normalized pigment chlorophyll ratio index			
4	TGI Triangular greenness index	$-0.5[(\lambda red - \lambda blue)(Rred - Rgreen) - (\lambda red - \lambda green)(Rred - Rblue)]$	UAV_RGB	Sentinel2A
5	VARI Visible atmospherically resistant index	$(Rgreen - Rred)/(Rgreen + Rred - Rblue)$	UAV_RGB	Sentinel2A
6	CIrededge Chlorophyll index – red-edge	$(Rnir/Rred\text{-}edge) - 1$	-	Sentinel2A
7	NDRE Normalized difference red-edge index	$(Rnir - Rred\text{-}edge)/(Rnir + Rred\text{-}edge)$	-	Sentinel2A
8	NDWI Normalized Difference Water Index	$(Rnir - Rswir)/(Rnir + Rswir)$	-	Sentinel2A
9	CIgreen Chlorophyll index – green	$(Rnir/Rgreen) - 1$	-	Sentinel2A
10	CVI Chlorophyll vegetation index	$Rnir(Rred/Rgreen2)$	-	Sentinel2A
11	EVI Enhanced vegetation index	$2.5(Rnir - Rred)/(Rnir + 6Rred - 7.5Rblue + 1)$	-	Sentinel2A
12	GNDVI Green normalized difference vegetation index	$(Rnir - Rgreen)/(Rnir + Rgreen)$	-	Sentinel2A
13	MCARI Modified chlorophyll absorption reflectance index	$[(Rred\text{-}edge - Rred) - 0.2(Rred\text{-}edge - Rgreen)](Rred\text{-}edge/Rred)$	-	Sentinel2A
14	MCARI2 Modified chlorophyll absorption reflectance index 2	$[1.5[2.5(Rnir - Rred) - 1.3(Rnir - Rgreen)]]/\sqrt{[(2Rnir + 1)2 - (6Rnir - 5\sqrt{Rred}) - 0.5]}$	-	Sentinel2A
15	MCARI_MTVI2 Combined index with MCARI	$MCARI/MTVI2$	-	Sentinel2A
16	MSAVI Modified soil adjusted vegetation index	$0.5\{2Rnir + 1 - \sqrt{[(2Rnir + 1)2 - 8(Rnir - Rred)]}\}$	-	Sentinel2A
17	MTCI MERIS terrestrial chlorophyll index	$(Rnir - Rred\text{-}edge)/(Rred\text{-}edge - Rred)$	-	Sentinel2A
18	NDVI Normalized difference vegetation index	$(Rnir - Rred)/(Rnir + Rred)$	-	Sentinel2A
19	MTVI2 Second modified triangular vegetation index	$1.5[2.5(Rnir - Rgreen) - 2.5(Rred - Rgreen)]/\sqrt{[(2\cdot Rnir + 1)2 - 6\cdot Rnir - 5\cdot\sqrt{(Rred)} - 0.5]}$	-	Sentinel2A
20	OSAVI Optimized soil adjusted vegetation index	$(1 + 0.16)(Rnir - Rred)/(Rnir + Rred + 0.16)$	-	Sentinel2A
21	SAVI Soil adjusted vegetation index	$(Rnir - Rred)(1 + 0.5)/(Rnir + Rred + 0.5)$	-	Sentinel2A

Proceedings of the 15th International Conference on Precision Agriculture
June 26-29, 2022, Minneapolis, Minnesota, United States

9

No.	Index	Formula		Sensor
22	**SR** **Ratio vegetation index (also named simple ratio)**	Rnir/Rred	-	Sentinel2A
23	**TCARI** **Transformed chlorophyll absorption reflectance index**	3[(Rred-edge – Rred) – 0.2(Rred-edge – Rgreen) (Rred-edge/Rred)]	-	Sentinel2A
24	**TCARI_OSAVI** **Combined index with TCARI**	TCARI/OSAVI	-	Sentinel2A
25	**TVI** **Triangular vegetation index**	0.5[120(Rnir − Rgreen) − 200(Rred − Rgreen)]	-	Sentinel2A
26	**VARIrededge** **Visible atmospherically resistant index-red-edge**	(Rred-edge − 1.7Rred + 0.7Rblue) / (Rred-edge + 2.3Rred − 1.3Rblue)	-	Sentinel2A

Proceedings of the 15th International Conference on Precision Agriculture
June 26-29, 2022, Minneapolis, Minnesota, United States

10